Beam-focus shaping by use of programmable phase-only filters: application to an ultralong focal line

B. Wattellier, C. Sauteret, J.-C. Chanteloup, and A. Migus

Laboratoire pour l'Utilisation des Lasers Intenses, Unité Mixte de Recherche 7605, Centre National de la Recherche Scientifique–Commissariat à l'Energie Atomique–Ecole Polytechnique–Université Paris 6, École Polytechnique, 91128 Palaiseau, France

Received August 10, 2001

We have developed a high-resolution programmable adaptive-optic device based on an optically addressed liquid-crystal electro-optic valve controlled by an achromatic three-wave lateral shearing interferometer. We apply this phase-only filter and loop to shape the far-field pattern of laser beams. As a first application, we theoretically compute and experimentally verify the focus along a line longer than tens of Rayleigh ranges.

OCIS codes: 140.3300, 100.5090, 160.3710.

The ability to control the shape of an intense laser is more and more important for laser–matter interaction. Shape control goes from the smallest possible spot, which is achieved through classical adaptive optics, to complex shapes such as ring patterns, long focal lines, or even more-complex profiles. In this regard, an adaptive-optic system was developed[1] that is based on an optically addressed liquid-crystal spatial light modulator, initially developed by Thales Research & Technology (TRT).[2] Here we use that system to create programmable phase-only filters (POFs). Because it is optically addressed, the modulator allows one to avoid the black matrix diffraction associated with electrically addressed pixelated devices, which decreases the contrast of the far-field patterns that are obtained. Furthermore, the system can operate in either an open or a closed loop (see Fig. 1). In the latter case, we measure the emergent wave front with an achromatic three-wave lateral shearing interferometer.[3] Both this sensor and the spatial light modulator have a high resolution (typically 100×100 control points).

In this Letter we describe the use of such a loop as a dynamic POF with the aim of producing a long focal line. A long focal line is of interest, for instance, in laser–plasma electron acceleration applications because it allows long acceleration lengths.[4] The 1-GeV energy range is expected to be reached with only 1-cm-long plasma.

It has been shown that our adaptive-optic loop proved to be efficient in correcting the distorted wave front of the Laboratoire l'Utilisation des Lasers Intenses (LULI) 300-fs 100-TW Nd:glass laser chain.[5] We verified that it could converge to predetermined arbitrary phase profiles with good accuracy. In particular, we studied the reproducability of our loop, especially with phase masks carrying high gradients. We reproduced several Zernike polynomial aberrations and verified, with a cw laser at first, that we were able to reproduce aberrations of higher than the sixth order with excellent accuracy (see Fig. 2).

We then used these masks for more-complex far-field patterns. For instance, in laser-plasma electron acceleration, it is known that the longer the plasma channel through which the accelerating laser propagates, the higher the output electron energy. Thus, we implemented a POF to shape the beam not only transversely but also along the optical axis.

To predetermine which phase mask would be optimum for that purpose, we used a ray-tracing method. Since the laser beam that we are dealing with has a diameter of 90 mm and is usually focused with a 700-mm off-axis parabola, the Rayleigh range at the focus spot is of the order of 80 μm. This is 2 orders of magnitude smaller than the focal range that we wanted to achieve ($\sim$1 cm), which justifies the use of geometrical optics. The main advantage of the method that we employed is that it allows one to find analytical solutions for the phase profile, assuming the paraxial approximation.

Since the focal has a cylindrical symmetry along the z axis (optical axis), we designed the POF with the same symmetry. The ray-tracing design (see Fig. 3) yields the wave vector in the POF plane. By integrating the radial component of this vector, we have access to the phase. We decided that the rays emerging from the center region of the beam had to converge at the beginning of the line and the outer rays at the end of the line. As soon as we know the power surface density, $I(r)$, in the near-field aperture and the power linear density in the focal region, $I(z)$, we can determine, by applying the energy-conservation law, the function linking the different points in these two regions: $z = f(r)$. This function yields the wave vectors and then the phase at the incident aperture.

For uniform incident and focal-line densities, the determination of this function is straightforward:

$$z(r) = f_1 + (f_2 - f_1)(r/R)^2, \quad (1)$$

where f_1 and f_2 are the beginning and the end of the focal line and R is the radius of the beam. Integrating the radial component of the deduced wave vectors, in the case of the paraxial approximation, leads to the following phase profile:

$$\varphi(r) = -\frac{2\pi}{\lambda}\frac{R^2}{2(f_2 - f_1)}\ln\left[1 + \frac{f_2 - f_1}{f_1}\left(\frac{r}{R}\right)^2\right]. \quad (2)$$

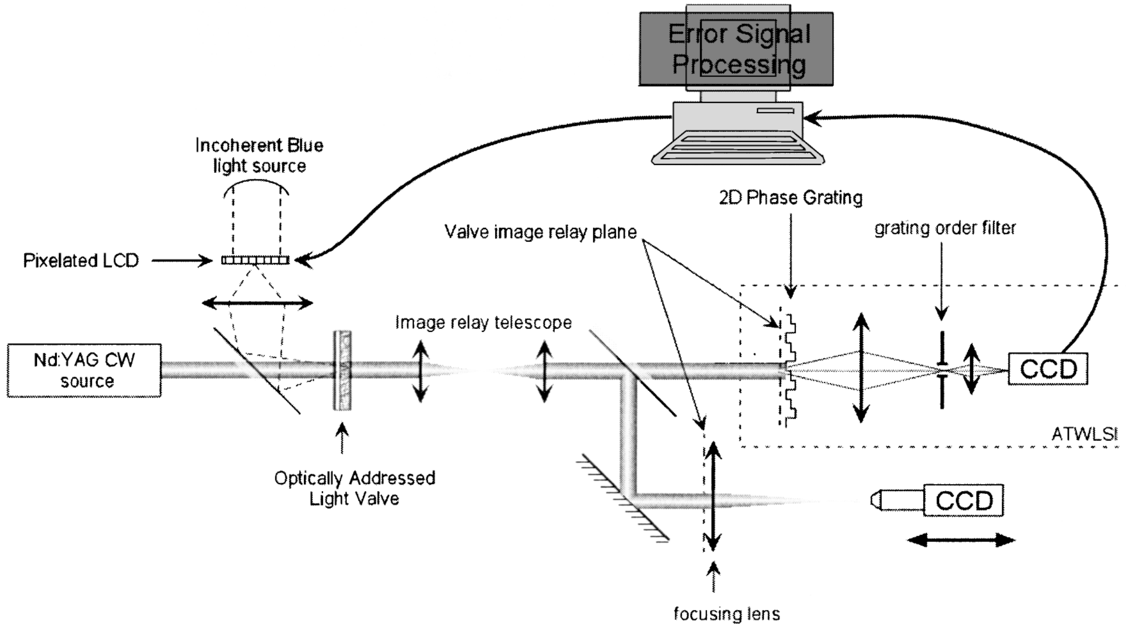

Fig. 1. Experimental setup for beam shaping. The liquid-crystal optically addressed spatial light modulator modifies the spatial phase that can be monitored by the achromatic three-wave lateral shearing interferometer (ATWLSI). The far-field pattern is imaged by a 10× microscope objective and recorded by a CCD camera. 2D, two-dimensional.

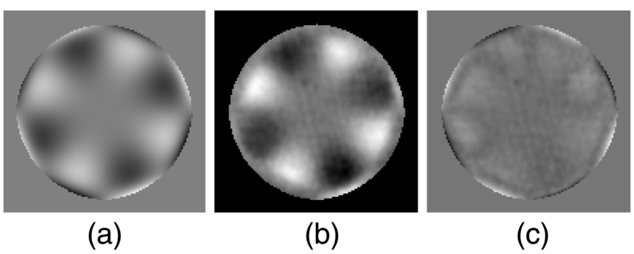

Fig. 2. Arbitrary phase-profile convergence. (a) We let the wave front coverage to ($n = 2$, $m = 4$) Zernike polynomial. (b) Measured wave front at the end of the loop. (c) Normalized error. The rms of the error is $\lambda/76$.

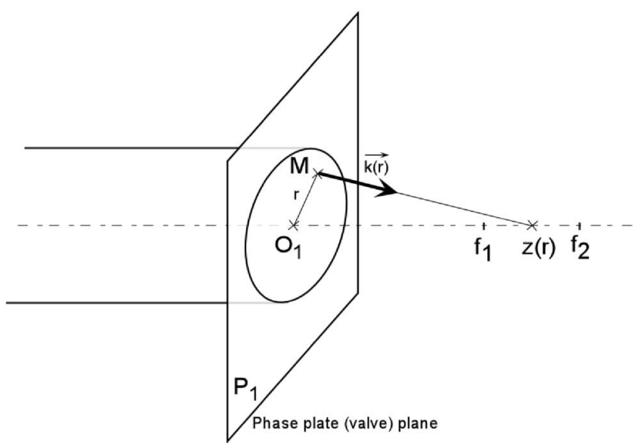

Fig. 3. Ray-tracing notation. A ray issuing from point M at radial coordinate r will intersect the optical axis at $z(r)$, located between f_1 and f_2, the extreme focus positions.

Actually, to apply this phase mask, we subtract this aberration from a thin lens, the focal length of which is optimized so that the phase shift in the phase profile is minimized:

$$f_{\mathrm{opt}} = \frac{f_1 + f_2}{2}\,. \tag{3}$$

For our case ($\lambda = 1057$ nm, $R = 45$ mm, $f_1 = 70$ cm, and $f_2 = 76$ cm), the maximum phase shift is 22λ. This kind of phase plate is obtainable by classical means (e.g., ion etching, holography).

We studied the pulse-energy deposition dynamics along the line with or without an additional lens. Since rays far from the optical axis focus at the end of the line, their optical path length is much longer than for rays close to the axis. For each ray, we can calculate the impact time $t(z)$ with the optical axis. We then defined the energy-deposition velocity, $v(z)$, by taking the first derivative of the reciprocal function $z(t)$:

$$\frac{v(z)}{c} = \frac{1}{c}\left(\frac{\partial t}{\partial z}\right)^{-1} \simeq 1 - \frac{f_1}{2(f_2 - f_1)}\left(\frac{R}{z}\right)^2. \tag{4}$$

We obtained a traveling wave whose speed can be slightly above or below c, depending on the sign of $f_2 - f_1$. Using a more rigorous analysis based on time-dependent diffraction,[6] we found that a 300-fs incident pulse results in a 300-fs pulse without significant broadening, propagating at $v(z)$ in the focal region. For the numerical application described above, the energy is deposited in ~200 ps if the whole phase is wrapped from 0 to 2π. If we consider using an additional lens to decrease the phase-shift range, we have to take into account the propagation time through the lens, which depends on the radial coordinate. This leads to another energy-deposition duration of 117 ps.

We now look at the pure spatial effect. Using the Fresnel approximation for the beam propagation, we

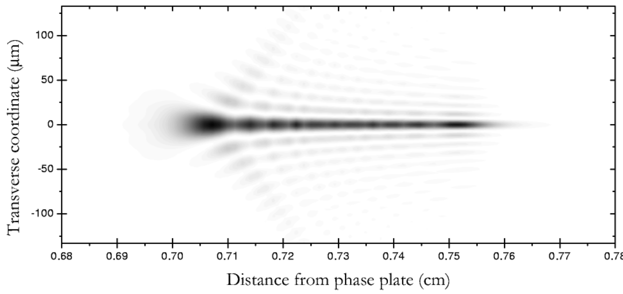

Fig. 4. Fresnel-diffraction-simulated focal region of the beam, focused with a phase plate designed to create a focal line. The line gets thinner and thinner at its end and is less than 50% of the diffraction limit for the same aperture in the near field.

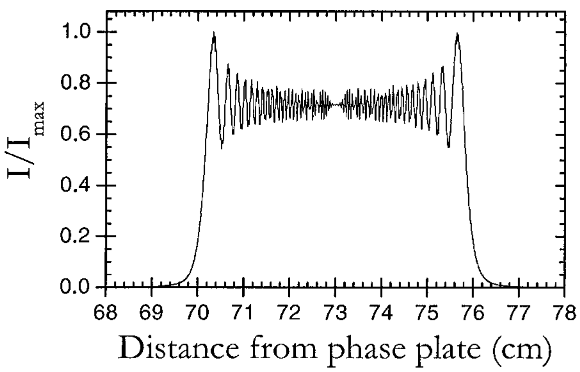

Fig. 5. Intensity along the optical axis, extracted from Fig. 4. The increase in intensity is sharp at the beginning and the end of the curve.

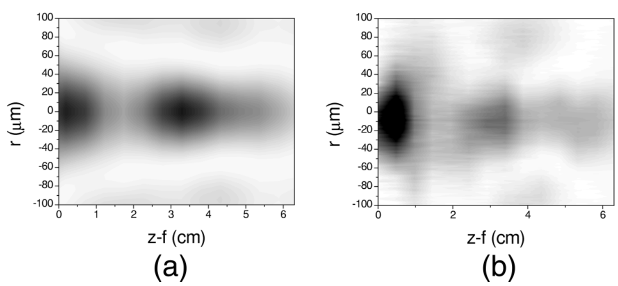

Fig. 6. Focal-spot regions of a beam modulated by a hologram producing a line of 6.3 cm. (a) Fresnel diffraction simulation. (b) Experiment: The intensity damping is due to the fact that the experimental beam was Gaussian.

simulated the electromagnetic field in the focal region (see Fig. 4). The intensity along the axis (see Fig. 5) is modulated by the diffraction of the flat-top input intensity. These modulations can be optically smoothed if the spectrum is large enough. However, the intensities at the beginning and the end of the line are the same.

The experimental results presented here (see Fig. 6) were obtained with a 100-mW Nd:YAG cw laser and the following parameters: $R = 3$ mm, $f_1 = 500$ mm, and $z_R = 9$ mm. We used the optimal computed lens to compensate for part of the applied phase mask. To apply the mask to the electro-optic valve, we also wrapped the residual phase to fit the liquid-crystal dynamics, which is less than three waves. The consequent local grating was not very dispersive, since it had only three periods in the radial direction. A 10× microscope objective with a CCD camera scanned the focal region of this lens. The obtained length of the line was $\Delta f = 6.3$ cm, that is, seven times the Rayleigh range. The line intensity is not uniform, because geometrical optics does not strictly apply in this case. We simulated the corresponding focal region [Fig. 6(a)] and found good agreement with the experimental measurement [Fig. 6(b)], considering that our laser had a Gaussian profile, which modulated the focal line.

In conclusion, we have shown that an adaptive-optic loop based on phase-only modulation by an optically addressed liquid crystal valve is efficient in shaping the far-field pattern of a laser beam. The shape of the beam is easily tunable by control of the mask applied to the valve. We studied the possibility of beam shaping in the longitudinal direction. Although this work was first motivated by the desire to control the geometry of laser–plasma interaction beams (e.g., x-ray laser pumping,[7] electron sources, accelerators), this method can find applications in low intensity and cw lasers in holography, data storage, and nonlinear optics. Furthermore, we are extending the method to create arbitrary far-field patterns, calculated by classical hologram-generation algorithms.[8] This approach allows us to generate, with low losses, alphanumerics, barcodes, or even gray-scale patterns, and applications in material processing (ablation, micromachining, photolithography, marking) are envisaged.

The authors thank J.-P. Huignard and B. Loiseaux of Thales TRT for providing the valve and for fruitful discussions concerning the low-intensity applications of the focal line. We also appreciate the discussions with V. Malka (LULI) about the relevance of beam shaping for plasma electron acceleration. This work was partly supported by grant E1127 from Region Ile-de-France. B. Wattellier's e-mail address is benoit.wattellier@polytechnique.org.

References

1. J. C. Chanteloup, H. Baldis, A. Migus, G. Mourou, B. Loiseaux, and J. P. Huignard, Opt. Lett. **23,** 475 (1998).
2. P. Aubourg, J.-P. Huignard, M. Hareng, and R. A. Mullen, Appl. Opt. **21,** 3706 (1982).
3. J. Primot, Appl. Opt. **32,** 6242 (1993).
4. A. Modena, Nature **377,** 606 (1995).
5. B. Wattellier, J. C. Chanteloup, J. Fuchs, C. Sauteret, J. P. Zou, and A. Migus, in *Conference on Lasers and Electro-Optics*, Vol. 56 of OSA Trends in Optics and Photonics Series (Optical Society of America, Washington, D.C., 2001), pp. 70–71.
6. Z. Bor, Opt. Lett. **14,** 119 (1989).
7. J. C. Chanteloup, E. Salmon, C. Sauteret, A. Migus, P. Zeitoun, A. Klisnick, A. Carillon, S. Hubert, D. Ros, P. Nickles, and M. Kalachnikov, J. Opt. Soc. Am. B **17,** 151 (2000).
8. R. W. Gerchberg and W. O. Saxton, Optik (Stuttgart) **35,** 237 (1972).